

DEFORMABLE MULTIBODY SYSTEMS WITH IMPACTS AND COULOMB FRICTION

Christian Maier* and Christoph Glocker*

*Institute of Mechanical Systems, Center of Mechanics
Department of Mechanical and Process Engineering, ETH Zurich, CH-8092 Zurich, Switzerland
e-mail: christian.maier@imes.mavt.ethz.ch,
e-mail: glocker@imes.mavt.ethz.ch,
web page: <http://www.zfm.ethz.ch/>

Keywords: FEM, non-smooth dynamics, impact, Coulomb friction, generalised force direction.

Abstract. *The aim of this paper is to present a discrete element approach for the investigation of deformable bodies combined with impacts and friction. Signorini's law and spatial isotropic Coulomb friction is assumed for the frictional unilateral contact. For the description of the impacts a Newton-type impact law is chosen. The value of the associated restitution coefficient is chosen in such a way, that a completely inelastic impact is obtained. This choice is explained by a 1D-model. Contact forces have to be expressed in the generalised degrees of freedom of the system, due to the integration into the equations of motion. For this approach generalised force directions are needed and calculated. The use of this method is shown with a 3D-model of which the bodies are discretised by trilinear hexahedral elements. This model description is used for investigations of the contact surface area changes, due to deformable bodies and friction.*

1 INTRODUCTION

The non-smooth contact dynamics approach has been developed during the last two decennia to describe systems, which consist of several bodies, with frictional unilateral constraints [2, 9]. For the modelling of a system with several bodies two possibilities exist: the rigid body and the continuum approach. Rigid body theory is often used for describing the dynamics of a multibody system. In continuum mechanics elastic or plastic responses of the structure are of interest due to external forces and momentums or prescribed deformations. These investigations are performed in the context of static or quasi-static analysis.

During the last years special attention is paid to develop a simulation tool in the area of non-smooth mechanical systems, which can treat also deformable bodies. In [1] a discrete element approach for the study of masonry is presented. Two different model types are used for the investigation: a rigid body modelling and a description of the system by a mechanical macroscopic tensor. The mechanical macroscopic tensor, which is called strain tensor, is defined on the background of granular media.

Another approach is to formulate the contact problem between several bodies for a continuum [8]. For a given configuration all contact constraints are described on the boundary of the bodies. In a further step the continuum approaches for the virtual contact work and its linearisation are discretised in space and time. Thus the term for the stiffness is achieved. This leads to a set of nonlinear equations of motion, which can be solved by a time-stepping algorithm.

The aim of this paper is to present a formulation of a finite element method for a dynamic simulation with deformable bodies including impact and friction. In the present work the collision between two deformable blocks is analysed. The approaches of the non-smooth mechanical system description are used, which contains impact equations, an impact law and Coulomb friction.

2 EQUATIONS OF MOTION

The principle of virtual work can be used for derivation of the equations of motion for a classical Lagrangian system. In [4] the procedure is shown on the basis of the principle of virtual power. For a holonomic system the equations of motion can also be derived with the principle of virtual work. This yields for the impact-free motion

$$\forall \delta \mathbf{q} : \quad 0 = \delta \mathbf{q}^T \left[\frac{d}{dt} \left(\frac{\partial T}{\partial \dot{\mathbf{q}}} \right)^T - \left(\frac{\partial T}{\partial \mathbf{q}} \right)^T + \left(\frac{\partial V}{\partial \mathbf{q}} \right)^T - \mathbf{f} \right]. \quad (1)$$

In Eq. (1) the time is described by t . The generalised coordinates of the multibody system with f degrees of freedom are denoted by $\mathbf{q} \in \mathbb{R}^f$. $\dot{\mathbf{q}}$ are the generalised velocities and $\delta \mathbf{q}$ the associated virtual displacements. The kinetic and potential energy of the holonomic system are denoted by $T(\dot{\mathbf{q}}, \mathbf{q})$ and $V(\mathbf{q})$, respectively. All generalised forces, which cannot be described by a potential, are summarised in \mathbf{f} . By differentiating and evaluating Eq. (1), the principle of virtual work is rewritten to

$$\forall \delta \mathbf{q} : \quad 0 = \delta \mathbf{q}^T [\mathbf{M}(\mathbf{q})\ddot{\mathbf{q}} - \mathbf{h}(\dot{\mathbf{q}}, \mathbf{q}) - \mathbf{f}], \quad (2)$$

with the symmetric and positive definite mass matrix $\mathbf{M}(\mathbf{q})$ and a f -tuple $\mathbf{h}(\dot{\mathbf{q}}, \mathbf{q})$ which contains the gyroscopic accelerations (Christoffel symbols) and the finite-valued generalised forces. Later the normal and tangential contact forces will be included in the f -tuple \mathbf{f} .

3 MODELLING OF IMPACT AND FRICTION

The following sections 3.1 and 3.2 will show a brief overview how contact problems can be modelled. These sections cover the contact model, contact laws and the impact law. Further and more detailed information can be found in [4, 5].

3.1 Contact model

For a contact model with friction the contact description consists of a gap function g_N , the relative velocities γ_i , $i \in \{N, B, C\}$ and the contact forces λ_i , $i \in \{N, B, C\}$. For a contact in \mathbb{R}^3 the indices N and B, C are the abbreviations for the normal direction and the two tangential directions, respectively. In Fig. (1) the left part depicts the kinematics of a two dimensional contact and the right graph shows the associated contact forces. The model (cf. Fig. 1) consists



Figure 1: 2D unilateral contact model with friction.

of two bodies and the possible pair of contact points P and Q (cf. [4, 5]). The outward normal unit vector at point P of the left body is $\mathbf{n}(\mathbf{q}) \in \mathbb{R}^3$. Let $\mathbf{r}_{PQ} \in \mathbb{R}^3$ be the connecting vector of the points P and Q . This vector denotes the relative displacement between the pair of contact points. The gap function is

$$g_N(\mathbf{q}) = \mathbf{n}^\top \mathbf{r}_{PQ} \quad (3)$$

in direction of normal vector \mathbf{n} , denominating the distance between P and Q . Both bodies touch each other in case of $g_N = 0$ at the points P and Q . For a value of $g_N > 0$ the contact is open and for a negative value the two bodies overlap or interpenetrate each other. Both interactions of the last case are forbidden and therefore excluded. This leads to an inequality constraint $g_N \geq 0$ for the distance between the pair of contact points. As \mathbf{r}_{PQ} is the relative displacement between the points P and Q , the relative velocity in normal direction γ_N between these points can be described by the time derivative of the gap function g_N (cf. [2])

$$\gamma_N = \mathbf{n}^\top (\mathbf{v}_Q - \mathbf{v}_P), \quad (4)$$

where \mathbf{v}_Q and \mathbf{v}_P denote the absolute velocities of point Q and P , respectively. The right part of Fig. 1 shows the free body diagram of the closed contact with friction at points P and Q . The contact forces at the points P and Q are divided into a force in normal direction $\mathbf{F}_{N*} \in \mathbb{R}^3$ and in tangential directions $\mathbf{F}_{B*} \in \mathbb{R}^3$ and $\mathbf{F}_{C*} \in \mathbb{R}^3$ with $*$ $\in \{P, Q\}$, which can be expressed by the corresponding vector of the contact coordinate system \mathbf{n} and \mathbf{b}, \mathbf{c} and a scalar force value λ_N and λ_B , respectively. Due to the principle of interaction the forces \mathbf{F}_{NP} and \mathbf{F}_{NQ} are equal, i.e. one scalar force value is adequate. For example the normal forces \mathbf{F}_{N*} can be rewritten

$$\begin{aligned} \mathbf{F}_{NP} &= -\lambda_N \mathbf{n} \\ \mathbf{F}_{NQ} &= \lambda_N \mathbf{n} \end{aligned} \quad (5)$$

by the unit normal vector \mathbf{n} and a scalar force value λ_N . Using Eq. (5) and the principle of virtual work the contact forces can be transformed into the generalised normal forces \mathbf{f}_N for the equations of motion

$$\mathbf{f}_N = \mathbf{w}_N \lambda_N \quad (6)$$

and included in Eq. (2). In Eq. (6) \mathbf{w}_N denotes the generalised force direction in normal direction (cf. chapter 6). Similar procedures are also applied for the tangential forces \mathbf{F}_{B^*} and \mathbf{F}_{C^*} . The necessary steps for the procedure are described in detail in [4]. The equations of motion Eq. (2), the contact forces $\mathbf{f}_N, \mathbf{f}_B, \mathbf{f}_C$ and the relative velocities $\gamma_N, \gamma_B, \gamma_C$ of the contact points in normal and tangential direction (cf. Eq. (6) and Eq. (4)) have to be completed by an impact law (e.g. Newton-type impact law) and force laws for the contact forces for a complete description of a f -dimensional dynamical system (cf. Fig. 1) with impacts.

3.2 Signorini's law and Coulomb friction

For the analysed model (cf. Fig. 5) Signorini's law and spatial isotropic Coulomb friction are used as force laws (cf. Fig. 2) for the modelling of unilateral contacts. The left graph of Fig. 2 shows Signorini's law, the right one depicts spatial isotropic Coulomb friction. Further force

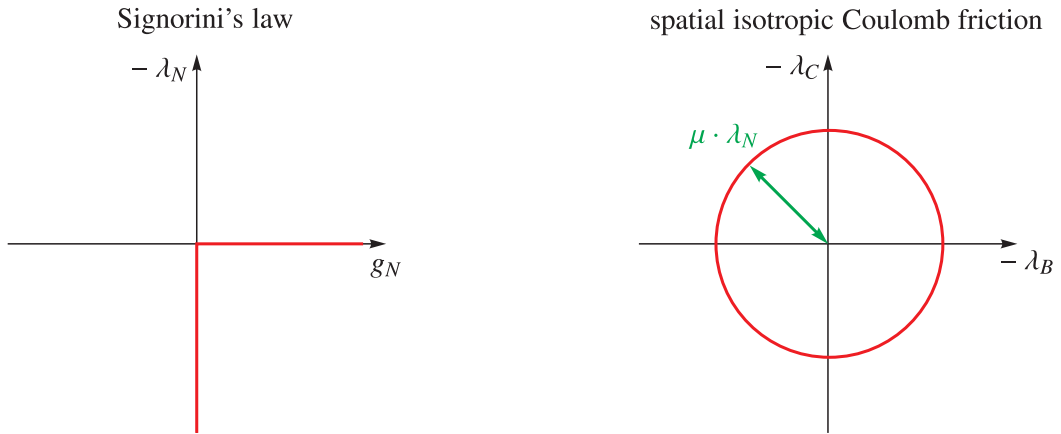


Figure 2: Signorini's law and spatial isotropic Coulomb friction.

laws are shown e.g. in [5]. For a unilateral contact it has to hold true, that only in state of a closed contact $g_N = 0$ normal and tangential forces λ_i , $i \in \{N, B, C\}$ can be transmitted. If the contact is open, the contact forces will vanish. This can be formulated for an open contact in normal direction as follows

$$g_N > 0 \Rightarrow \lambda_N = 0 \quad (7)$$

and for a closed contact in normal direction

$$g_N = 0 \Rightarrow \lambda_N \geq 0. \quad (8)$$

The expressions in Eq. (7) and Eq. (8) can be represented by the normal cone inclusion [5]

$$g_N \in \mathcal{N}_{\mathbb{R}_0^-}(-\lambda_N). \quad (9)$$

Assuming that the contact is closed the tangential contact forces \mathbf{F}_B and \mathbf{F}_C can be represented by the tangential vectors \mathbf{b} , \mathbf{c} of the contact coordinate system and a scalar force value λ_B and λ_C , respectively. For the given constellation at point P (cf. fig. 1 extended for three dimensions), the two tangential contact forces \mathbf{F}_B and \mathbf{F}_C

$$\mathbf{F}_B = -\lambda_B \mathbf{t} \quad (10)$$

$$\mathbf{F}_C = -\lambda_C \mathbf{b} \quad (11)$$

can be reformulated in the same way as the normal direction (cf. Eq. (5)). For an open contact ($g_N > 0$) the following correlation must be fulfilled:

$$g_N > 0 \Rightarrow -\lambda_B = 0 \wedge -\lambda_C = 0. \quad (12)$$

Is a frictional contact closed, two cases have to be distinguished: Sliding and sticking. The right part in Fig. 2 shows the force law of spatial isotropic Coulomb friction. In case of sliding the possible values of the friction forces are displayed on the boundary of the circle, with radius $\mu \cdot \lambda_N$. The boundary and the area of the circle represent the set of the possible values of the friction force $\boldsymbol{\lambda}_T = (\lambda_B, \lambda_C)^\top$ in case of sticking. The friction force $\boldsymbol{\lambda}_T$ is determined by two correlations, an equation in case of sliding and an inequality constraint for a vanished relative velocity $\boldsymbol{\gamma}_T = (\gamma_B, \gamma_C)^\top$

$$g_N = 0 \Rightarrow \begin{cases} \boldsymbol{\gamma}_T \neq 0 \Rightarrow -\boldsymbol{\lambda}_T = \mu \lambda_N \mathbf{e}_T(\boldsymbol{\gamma}_T) \\ \boldsymbol{\gamma}_T = 0 \Rightarrow \|\boldsymbol{\lambda}_T\| \leq \mu \lambda_N \end{cases}, \quad (13)$$

with sliding direction $\mathbf{e}_T(\boldsymbol{\gamma}_T) = \frac{\boldsymbol{\gamma}_T}{\|\boldsymbol{\gamma}_T\|}$. The force law of Eq. (13) can be rewritten as a normal cone inclusion

$$g_N = 0 \Rightarrow \boldsymbol{\gamma}_T \in \mathcal{N}_{C_T}(-\boldsymbol{\lambda}_T), \quad (14)$$

with the set C_T

$$C_T = \{\boldsymbol{\lambda}_T \in \mathbb{R}^2 \mid \|\boldsymbol{\lambda}_T\| \leq \mu \lambda_N\}. \quad (15)$$

The coefficient of friction is a scalar for spatial isotropic Coulomb friction. The needed force laws for modelling the unilateral normal contact is given in Eq. (9) and for the closed contact with friction in Eq. (14) and Eq. (15), respectively.

4 MODEL DESCRIPTION

For the analysis of a 3D-model with impacts two deformable bodies are used. As restitution coefficient $\varepsilon = 0$ is chosen, that means a completely inelastic impact in terms of a Newton-type impact law. For a system consisting of two continua, which are modelled as non-dissipative, and impacts with a restitution coefficient $\varepsilon = 0$ energy conservation is fulfilled [3]. After a spacial discretisation of a continuum, e.g. with a finite element approach, and the identical impact coefficient $\varepsilon = 0$ the total energy is no longer preserved. This results from the spatial discretisation of the continuum, because the continuous mass is distributed to a finite number of degrees of freedom of the system. The dynamical behaviour of this system is similar to a rigid body system consisting of point masses which are connected by springs. The loss of energy and the choice of the restitution coefficient value can be explained with a one-dimensional model, which is done in the following section.

4.1 1D-Model

The rationale for choosing a completely inelastic impact law, i.e. a restitution coefficient $\varepsilon = 0$, is explained by a one-dimensional model shown in Fig. 4. The required contact quantities are shown in Fig. 3. Consider a rigid wall and two point masses m_1 and m_2 , which are connected



Figure 3: 1D-model with impact kinematics.

by a linear spring with stiffness k . The spring is unstressed during the following kinematic considerations. The left part of Fig. 3 shows the system during an impact-free motion. The contact is defined between the rigid wall, which is fixed inertially, and the point mass m_1 . The corresponding position and relative velocity of point mass m_1 is depicted in the right part of Fig. 3. The position of point mass m_1 is described by the coordinate x_1 . The gap function g_N between the point mass and the rigid wall is in general, and applied for the given 1D-case

$$g_N = \mathbf{n}^T \mathbf{x}, \quad g_N = x_1. \quad (16)$$

As shown in [2] the relative velocity in normal direction is the time derivative of the normal gap function $\gamma_{N_i} = \dot{g}_{N_i}$. At the instant of collision the contact is closed and the relative post impact velocity can be calculated by an impact law e.g. Newton-type one

$$\gamma_N^+ = -\varepsilon \gamma_N^-. \quad (17)$$

The Newton-type impact law (cf. Eq. (17)) presents a correlation in normal direction between a relative pre-impact velocity γ_N^- and a relative post-impact velocity γ_N^+ via the coefficient of restitution ε . In case of a completely inelastic impact law ($\varepsilon = 0$) the value of the relative post-impact velocity is zero. Due to the fact that the rigid wall is fixed inertially, the relative velocity between the two contact partners is identical to the absolute velocity of the point mass m_1 . For a coefficient of restitution $\varepsilon = 0$ the relative post-impact velocity γ_N^+ is zero, independently from the relative pre-impact velocity γ_N^- . This means, that the relative velocity γ_N vanishes after the impact and the contact remains closed, because the absolute velocity of point mass m_1 is zero. The pre-impact kinetic energy T^- of point mass m_1 is non-zero and the post-impact kinetic energy T^+ of the point mass m_1 is zero. The difference between the kinetic energies $T^+ - T^-$ corresponds to the loss of the total energy for a system with impacts. The system without impacts is modelled as a non-dissipative one in the approach of classical mechanics. These facts influence the dynamics of the system and the consequences will be explained with the same mechanical 1D-example (cf. Fig. 4) as shown in Fig. 3. Initially the spring with stiffness k is unstressed and the point masses m_1 and m_2 approach the rigid wall with the same initial velocity of $-v$ (cf. Fig. 4a). The point mass m_1 hits the wall and is instantaneously decelerated to zero velocity because of a completely inelastic impact law (cf. Eq. (17) with $\varepsilon = 0$), whereas the point mass m_2 moves uninfluenced with initial velocity $-v$ (cf. Fig. 4b). Therefore, the spring is compressed and point mass m_2 decelerates transforming its kinetic energy to the potential energy of the spring. After decelerating point mass m_2 to zero velocity (cf. Fig. 4c), it

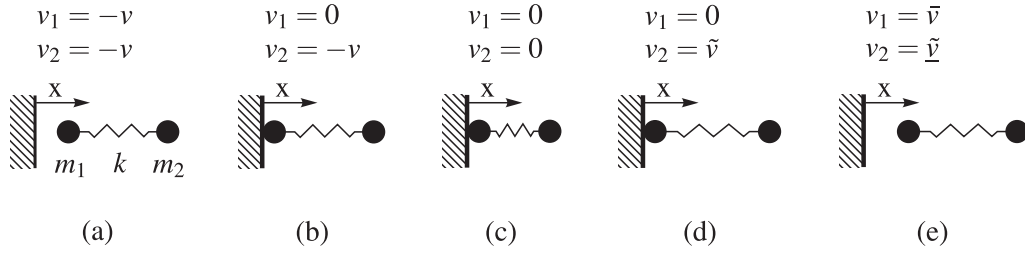


Figure 4: One-dimensional model for explanation of the restitution coefficient value.

is accelerated by retransforming the potential energy of the spring to kinetic energy of point mass m_2 (cf. Fig. 4d). Because of the inertia of the accelerated point mass m_2 , point mass m_1 is accelerated and lifts off from the wall (cf. Fig. 4e). Hence, a completely inelastic impact law is sufficient to explain the rebounding of colliding deformable bodies and implies that the bodies remain in contact during collision.

4.2 3D-Model

The dynamical behaviour of the one-dimensional model (cf. Fig. 4) and the analysed model (cf. Fig. 5) are comparable, but it deforms in all spatial directions and has frictional unilateral constraints. The 3D-model, which is used for the analysis, consists of two deformable bodies, a cuboid and a cube. Each block is described by a trilinear hexahedral element [7]. The cube is

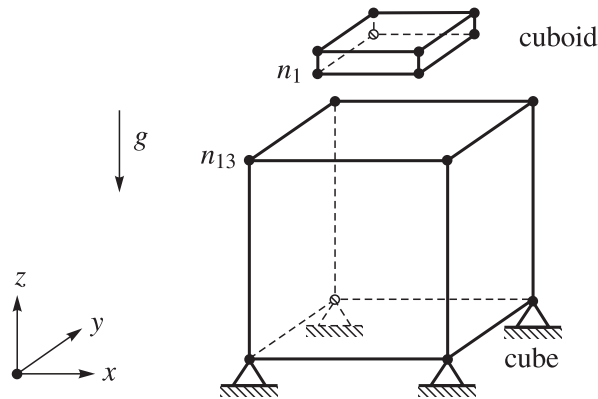


Figure 5: Sketch of the 3D-model.

fixed at the four lower nodes (cf. Fig. 5). Initially the cuboid is completely unconstrained until it collides with the cube. The contact between the cuboid and the cube are defined as node-to-surface contacts, i.e. the four bottom nodes of the cuboid (e.g. node n_1) can come into contact with the upper surface of the cube. A frictional unilateral behaviour of the contacts is assumed: Signorini's law in normal direction, spatial isotropic Coulomb friction law in tangential directions and a frictional Newton-type impact law. The material behavior is modelled linear elastic for both bodies [12].

5 CONTACT FORCE REDUCTION

Different kinds of discretisations, as it is provided by the finite element method [7, 12], are used for continua. After the discretisation of the continuum, forces cannot interact with

the body at every arbitrary point, but forces can only be applied as generalised forces. These forces have the dimension f and they are the transformed arbitrary applied forces, with f the number of generalised degrees of freedom of the system. Therefore and due to the different geometrical dimensions of the contact partners (cf. Fig. 5) a node-to-surface contact definition is used. The upper surface area of the cube is greater than the bottom area of the cuboid, thus the contact forces applied on the cube surface have to be distributed to the upper nodes of the cube (cf. Fig. 5 e.g. node n_{13}). Interaction of a contact force with the cube is comparable to an arbitrary applied force at a discretised model. A cube with an arbitrary applied force \mathbf{F}_P

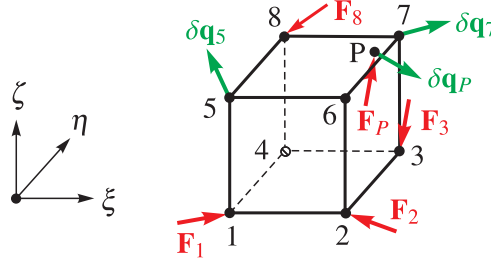


Figure 6: Generalised nodal forces $\mathbf{F}_1, \mathbf{F}_2, \dots, \mathbf{F}_8$ of the applied force \mathbf{F}_P .

at P with coordinates $\mathbf{p} = (\xi_P, \eta_P, \zeta_P)^\top$ in local element coordinates is shown in Fig. 6. A trilinear hexahedral element [7] is chosen as finite element. At the cube corners the nodes of the discretised model are situated. With the invariance of the principle of virtual work, the force \mathbf{F}_P is transformed to the corner node forces \mathbf{F}_i , also called the generalised forces. The virtual work of the arbitrary applied external force \mathbf{F}_P at P is

$$\delta W_P = \mathbf{F}_P^\top \delta \mathbf{q}(\mathbf{p}), \quad (18)$$

where $\delta \mathbf{q}(\mathbf{p}) = \delta \mathbf{q}_P$ is the virtual displacement at point P . The virtual work of the corner node forces \mathbf{F}_i can be calculated as follows

$$\delta W_i = \sum_{i=1}^8 \mathbf{F}_i^\top \delta \mathbf{q}_i, \quad (19)$$

with the virtual displacements at the nodes i , which are denoted as $\delta \mathbf{q}_i$. Displacement vector \mathbf{q} at an arbitrary point of the cube is a function

$$\mathbf{q} = \mathbf{q}(\xi, \eta, \zeta, N_i(\xi, \eta, \zeta)), \quad i \in \{1, 2, 3, \dots, 8\} \quad (20)$$

of the local element coordinates and the shape functions $N_i(\xi, \eta, \zeta)$ of the cube, which are used for the discretisation of the block and which are on their part a function of the local element coordinates, too. Now, the shape functions will not be displayed anymore with the local element coordinate dependence. Displacement of an arbitrary point of the cube can be described as a function of the displacements of each node. Thus the virtual displacement of point P can be calculated as follows:

$$\delta \mathbf{q}_P = \sum_{i=1}^8 \left. \frac{\partial}{\partial \mathbf{q}_i} \mathbf{q}(\xi, \eta, \zeta, N_i) \right|_P \delta \mathbf{q}_i, \quad (21)$$

with the displacement \mathbf{q}_i at node i . After calculating the derivative of the displacement vector \mathbf{q} it is evaluated at point P. The virtual work of \mathbf{F}_P can be expressed with Eq. (18) and Eq. (21) in terms of the displacement vector \mathbf{q} and the virtual displacements of the nodes i

$$\delta W_P = \mathbf{F}_P^\top \sum_{i=1}^8 \frac{\partial}{\partial \mathbf{q}_i} \mathbf{q}(\xi, \eta, \zeta, N_i) \Big|_P \delta \mathbf{q}_i. \quad (22)$$

The virtual work δW_P of an arbitrary external force \mathbf{F}_P and the virtual work δW_i of the generalised forces \mathbf{F}_i must be equal $\delta W_P \equiv \delta W_i$. This correlation yields to

$$\mathbf{F}_P^\top \sum_{i=1}^8 \frac{\partial}{\partial \mathbf{q}_i} \mathbf{q}(\xi, \eta, \zeta, N_i) \Big|_P \delta \mathbf{q}_i \equiv \sum_{i=1}^8 \mathbf{F}_i^\top \delta \mathbf{q}_i. \quad (23)$$

The virtual displacements in Eq. (23) are identical and thus the forces \mathbf{F}_i at node i can be calculated as

$$\mathbf{F}_i = \frac{\partial}{\partial \mathbf{q}_i} \mathbf{q}(\xi, \eta, \zeta, N_i) \Big|_P \mathbf{F}_P. \quad (24)$$

A Galerkin approach with shape functions N_i is used for the discretisation of the bodies

$$N_i(\xi, \eta, \zeta) = \frac{1}{8} (1 + \xi_a \xi) (1 + \eta_a \eta) (1 + \zeta_a \zeta), \quad (25)$$

with the nodal coordinates ξ_a, η_a and ζ_a (cf. [7]). The calculus of the derivative and the evaluation of the derivative at point P in Eq. (24) yields together with Eq. (25)

$$\mathbf{F}_i = (N_i(\mathbf{p}) \cdot \mathbf{1}) \mathbf{F}_P, \quad (26)$$

with the identity matrix $\mathbb{R}^{3,3}$. A correlation for the calculation of the generalised forces \mathbf{F}_i due to an arbitrary applied force \mathbf{F}_P is given in Eq. (26).

6 CALCULATION OF THE GENERALISED FORCE DIRECTIONS

The generalised force directions are needed for the integration of the contact forces λ_k with $k \in \{N, B, C\}$ in normal direction N and the two tangential directions B and C , respectively, into the equations of motion [2]. Generalised force directions have the dimension $\mathbb{R}^{f,n}$, where f denotes the number of degrees of freedom of the system and n is the number of the contact points. Fig. 7 shows the free body diagram of the two bodies in contact (cf. a part of Fig. 5). The contact forces of the cuboid are depicted at the node n_1 and at the interaction point on the surface of the cube (cf. Fig. 7). A local contact coordinate system is specified for the cuboid $l = 1$ and for the cube $l = 2$. Let \mathbf{n}_l be the normal direction of the contact and $\mathbf{b}_l, \mathbf{c}_l$ the two tangential directions. The coordinate systems are not illustrated at the contact points, because they are more clearly presented at other nodes. The origin of the coordinate system (index l) is placed at the corresponding point of each contact point of the blocks (cf. Fig. (7)). The contact force in normal direction is represented by $\mathbf{F}_{N_{nm}}$, the tangential forces based on friction by $\mathbf{F}_{B_{nm}}, \mathbf{F}_{C_{nm}}$, where n is the abbreviation for node and index m is numbered consecutively, i.e. odd indices for the cuboid and even ones for the cube. The contact forces on the surface of the cube have to be transformed to the neighbouring nodes, i.e. nodes n_{13} to n_{16} (cf. Fig. (7)), applying the

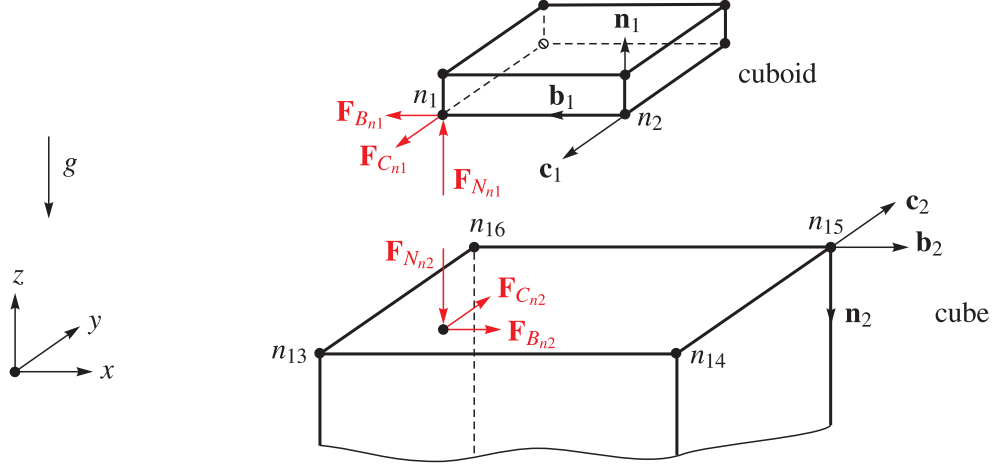


Figure 7: Contact forces between the cube and the cuboid.

approach from section 5. The contact forces may be expressed by the local contact coordinate system \mathbf{n}_l , \mathbf{b}_l and \mathbf{c}_l and a corresponding scalar force value $\lambda_{N_{nm}}$, $\lambda_{B_{nm}}$ and $\lambda_{C_{nm}}$, respectively,

$$\begin{aligned} \mathbf{F}_{N_{n1}} &= \lambda_{N_{n1}} \mathbf{n}_1, & \mathbf{F}_{N_{n2}} &= \lambda_{N_{n2}} \mathbf{n}_2, \\ \mathbf{F}_{B_{n1}} &= \lambda_{B_{n1}} \mathbf{b}_1, & \mathbf{F}_{B_{n2}} &= \lambda_{B_{n2}} \mathbf{b}_2, \\ \mathbf{F}_{C_{n1}} &= \lambda_{C_{n1}} \mathbf{c}_1, & \mathbf{F}_{C_{n2}} &= \lambda_{C_{n2}} \mathbf{c}_2. \end{aligned} \quad (27)$$

According to the principle of interaction the normal forces $\mathbf{F}_{N_{nm}}$ and the tangential forces $\mathbf{F}_{B_{nm}}$, $\mathbf{F}_{C_{nm}}$ are opposite to each other and their absolute values are identical. This means for the contact forces at the contact point of node n_1

$$\begin{aligned} \mathbf{F}_{N_{n1}} &= -\mathbf{F}_{N_{n2}} = \lambda_{N_{n1}} \mathbf{n}_1 = -\lambda_{N_{n1}} \mathbf{n}_2, \\ \mathbf{F}_{B_{n1}} &= -\mathbf{F}_{B_{n2}} = \lambda_{B_{n1}} \mathbf{b}_1 = -\lambda_{B_{n1}} \mathbf{b}_2, \\ \mathbf{F}_{C_{n1}} &= -\mathbf{F}_{C_{n2}} = \lambda_{C_{n1}} \mathbf{c}_1 = -\lambda_{C_{n1}} \mathbf{c}_2. \end{aligned} \quad (28)$$

Now, the scalar force values are abbreviated by λ_{k_j} , where j denotes the contact number and k the direction

$$\begin{aligned} \mathbf{F}_{N_{n1}} &= -\mathbf{F}_{N_{n2}} = \lambda_{N_1} \mathbf{n}_1 = -\lambda_{N_1} \mathbf{n}_2, \\ \mathbf{F}_{B_{n1}} &= -\mathbf{F}_{B_{n2}} = \lambda_{B_1} \mathbf{b}_1 = -\lambda_{B_1} \mathbf{b}_2, \\ \mathbf{F}_{C_{n1}} &= -\mathbf{F}_{C_{n2}} = \lambda_{C_1} \mathbf{c}_1 = -\lambda_{C_1} \mathbf{c}_2. \end{aligned} \quad (29)$$

The contacts are numbered with the corresponding node index of the nodal part of the node-to-surface contact definition. Two things are needed for the integration of the contact forces into the equations of motion: the scalar force values (cf. Eq. (29)) and the generalised force directions. The generalised force directions have to be calculated as shown in [5]. They consists of two parts: the index one part is related to the cuboid and the index two summand to the cube

$$\begin{aligned} \mathbf{w}_N &= (\mathbf{Q}_1 - \mathbf{Q}_2)^\top \mathbf{n}, \\ \mathbf{w}_B &= (\mathbf{Q}_2 - \mathbf{Q}_1)^\top \mathbf{b}, \\ \mathbf{w}_C &= (\mathbf{Q}_2 - \mathbf{Q}_1)^\top \mathbf{c}. \end{aligned} \quad (30)$$

\mathbf{w}_k has the dimension $\mathbb{R}^{f,1}$, with f the number of generalised degrees of freedom of the system. The generalised force direction vectors \mathbf{w}_k for contact j transform the contact forces $\mathbf{F}_{k_{nj}}$ into

the generalised force vector \mathbf{f} , which is a part of the equations of motion. The contact forces of the nodal part of the contact definition (cf. Fig. 7 e.g. node n_1) do not have to be transformed. The interaction forces on the upper surface of the cube of the nodal contact forces, e.g. at the corresponding contact point of node n_1 on the cube surface, have to be transformed to the nodes n_{13} up to n_{16} (cf. Fig. 7). The Jacobi matrix $\mathbf{Q}_{j_1} \in \mathbb{R}^{3,f}$, with f generalised system degrees of freedom and the three dimensions of the 3-tupel of the contact force $vF_{k_{nj}}$, for the contact force at node n_j of the cuboid is

$$\mathbf{Q}_{j_1} = \begin{pmatrix} 0 & \dots & 0 & 1 & 0 & 0 & 0 & \dots & 0 \\ 0 & \dots & 0 & 0 & 1 & 0 & 0 & \dots & 0 \\ 0 & \dots & 0 & 0 & 0 & 1 & 0 & \dots & 0 \end{pmatrix}, \quad (31)$$

$\underbrace{\hspace{10em}}_{\in \mathbb{R}^{3,n}} \quad \underbrace{\hspace{10em}}_{\in \mathbb{R}^{3,3}} \quad \underbrace{\hspace{10em}}_{\in \mathbb{R}^{3,m}}$

where the identity matrix is located at the same position as the coordinates of the cuboid node n_j in the vector of the generalised coordinates \mathbf{q}

$$\mathbf{q}^\top = \left(\underbrace{* \dots *}_{\in \mathbb{R}^{1,n}} \quad \underbrace{\mathbf{r}_{j_x} \quad \mathbf{r}_{j_y} \quad \mathbf{r}_{j_z}}_{\in \mathbb{R}^{1,3}} \quad \underbrace{* \dots *}_{\in \mathbb{R}^{1,m}} \right). \quad (32)$$

The coordinates of node n_j are described by \mathbf{r}_{j_x} , \mathbf{r}_{j_y} and \mathbf{r}_{j_z} . The second part of the generalised force directions in Eq. (30), which derives from the Jacobi matrix \mathbf{Q}_2 and the corresponding vector of the contact coordinate system, is calculated in the same manner as the reduction of the contact forces (cf. chapter 5). The following correlation can be formulated for each contact force $\mathbf{F}_{k_{nm}}$, which is located on the surface of the cube, e.g. m is a even number

$$\mathbf{Q}_{j_2} = \left(0 \quad \dots \quad 0 \quad N_{13}(\mathbf{p}_j) \cdot \mathbb{1} \quad N_{14}(\mathbf{p}_j) \cdot \mathbb{1} \quad N_{15}(\mathbf{p}_j) \cdot \mathbb{1} \quad N_{16}(\mathbf{p}_j) \cdot \mathbb{1} \right), \quad (33)$$

where N_i denotes the corresponding shape functions of node i of the cube $i \in \{13, 14, 15, 16\}$ (cf. Fig.7). The product of the identity matrix and the shape function N_i is assembled in the Jacobi matrix \mathbf{Q}_{j_2} at the position of the corresponding coordinates of node n_{13} up to n_{16} in the vector of generalised coordinates \mathbf{q} . The generalised force directions \mathbf{w}_k are calculated as described in [2] for every single contact j

$$\begin{aligned} \mathbf{w}_{N_j} &= (\mathbf{Q}_{j_1} - \mathbf{Q}_{j_2})^\top \mathbf{n}, \\ \mathbf{w}_{B_j} &= (\mathbf{Q}_{j_2} - \mathbf{Q}_{j_1})^\top \mathbf{b}, \\ \mathbf{w}_{C_j} &= (\mathbf{Q}_{j_2} - \mathbf{Q}_{j_1})^\top \mathbf{c}. \end{aligned} \quad (34)$$

For each contact point j the contact forces $\mathbf{F}_{N_{nm}}$, $\mathbf{F}_{B_{nm}}$, $\mathbf{F}_{C_{nm}}$ are integrated into the equations of motion Eq. (2) with a scalar force value λ_{N_j} , λ_{B_j} , λ_{C_j} (cf. Eq. (29)) and the corresponding generalised force directions \mathbf{w}_{N_j} , \mathbf{w}_{B_j} , \mathbf{w}_{C_j} (cf. Eq. (34)). For a closed contact at node n_1 (cf. Fig.7) the contact forces are added to the equations of motion Eq. (2) with the f -tupel \mathbf{f} ,

$$\mathbf{f} = \mathbf{w}_{N_1} \lambda_{N_1} + \mathbf{w}_{B_1} \lambda_{B_1} + \mathbf{w}_{C_1} \lambda_{C_1}. \quad (35)$$

If more contacts are closed the generalised force directions will be collected conveniently in the corresponding directions N, B, C to the generalised force matrices \mathbf{W}_N , \mathbf{W}_B and \mathbf{W}_C . In the same way the scalar contact forces are summarised in a contact forces vector in the different directions λ_N , λ_B and λ_C , respectively.

7 TIME DISCRETISATION

The equations of motion are solved with the so-called time-stepping algorithm by Moreau [11]. This method uses an explicit midpoint rule for the positions and an implicit Euler backward step on velocity level. For a chosen time interval $[t^A, t^E]$ the time discretisation is shown in Fig. 8. The position at the beginning of every time step $\mathbf{q}^A := \mathbf{q}(t^A)$ and the corresponding initial velocity $\mathbf{u}^A := \mathbf{u}(t^A)$ are known. The approximate solutions at endpoint t^E are positions $\mathbf{q}^E := \mathbf{q}(t^E)$ and velocities $\mathbf{u}^E := \mathbf{u}(t^E)$, which are calculated from the initial conditions. The position $\mathbf{q}^M := \mathbf{q}(t^M)$ at time t^M is guessed with an explicit Euler step. If all

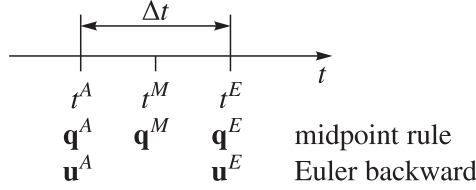


Figure 8: Time discretisation after [5].

frequencies of an investigated system have to be represented, a small time step Δt is required. This corresponds to high computational effort. A reduction of calculation time can be achieved by using an implicit integrator. The use of a greater time step Δt is the reason of the decreasing computation time. This choice of the time step size is possible due to the characteristics of an implicit integrator: numerical damping and neglecting higher frequencies. In the scope of this paper only lower frequencies are of interest and an implicit integrator can be used. Two different discretisations and the appropriate numerical implementation are used for showing the influence of the integrator choice. As basis for the investigation of the system, which consists of two deformable bodies with impacts and friction, the time-stepping algorithm of Moreau [11] is used. The calculation of the midpoint position \mathbf{q}^M and the position at the end of the time step \mathbf{q}^E is adjusted to an energy consistent integrator and accordingly to an implicit one, respectively. These changes are described in the following sections.

7.1 Energy consistent integrator

During the instant of collision energy is dissipated because of the spacial discretisation and the chosen Newton-type impact law with the associated coefficient of restitution $\varepsilon = 0$. For deformable bodies with impacts the loss of energy shall be limited to the instant of collision. For this reason an energy consistent integrator as developed in [10] is chosen. The generalised force direction and the contact forces (cf. Eq. (35)) are taken into account in the equations of motion

$$\mathbf{M}\ddot{\mathbf{u}} - \mathbf{h}(\mathbf{u}, \mathbf{q}) - \mathbf{W}_N \boldsymbol{\lambda}_N - \mathbf{W}_T \boldsymbol{\lambda}_T - \mathbf{W}_B \boldsymbol{\lambda}_B = 0, \quad (36)$$

for the chosen generalised coordinates the mass matrix \mathbf{M} is constant. In a first step Eq. (36) is transformed to a discrete form as described in [5, 6]:

$$\mathbf{M}(\mathbf{u}^E - \mathbf{u}^A) - \mathbf{h}(\mathbf{u}^A, \mathbf{q}^M, t) \Delta t - \mathbf{W}_N \mathbf{P}_N - \mathbf{W}_T \mathbf{P}_T - \mathbf{W}_B \mathbf{P}_B = 0, \quad (37)$$

with \mathbf{P}_k the percussion of the contact forces. The midpoint position \mathbf{q}^M is defined as

$$\mathbf{q}^M := \mathbf{q}^A + \frac{1}{4} \Delta t (\mathbf{u}^A + \mathbf{u}^E). \quad (38)$$

The closed contacts j are identified and its corresponding generalised force vectors $\mathbf{w}_{N_j}, \mathbf{w}_{B_j}$ and \mathbf{w}_{C_j} are collected in the generalised force direction matrices $\mathbf{W}_N, \mathbf{W}_B$ and \mathbf{W}_C , respectively. That means that only the closed contacts are considered in the equations of motion. In the following the inclusion problem

$$\begin{aligned} \mathbf{M}(\mathbf{u}^E - \mathbf{u}^A) - \mathbf{h}\Delta t - \mathbf{W}_N \mathbf{P}_N - \mathbf{W}_T \mathbf{P}_T - \mathbf{W}_B \mathbf{P}_B &= 0 \\ \text{with: } \mathbf{h} &= \mathbf{K}(\mathbf{q}^A + \frac{\Delta t}{4}(\mathbf{u}^A + \mathbf{u}^E) - \mathbf{q}_0) \\ \gamma_{k_j}^A &= \mathbf{w}_{k_j}^\top \mathbf{u}^A + \chi_{k_j}, \quad \gamma_{k_j}^E = \mathbf{w}_{k_j}^\top \mathbf{u}^E + \chi_{k_j} \\ \gamma_{N_j}^E + \varepsilon_{N_j} \gamma_{N_j}^A &\in \mathcal{N}_{\mathbb{R}_0^-}(-P_{N_j}) \\ \gamma_{T_j}^E + \boldsymbol{\varepsilon}_{T_j} \gamma_{T_j}^A &\in \mathcal{N}_{C_T}(-\mathbf{P}_{T_j}) \end{aligned} \quad (39)$$

is solved (cf. [5, 6]). Where $\mathbf{P}_{T_j} = (P_{B_j}, P_{C_j})^\top$ denotes the tangential contact forces of contact j , the restitution coefficient in normal direction is represented by ε_{N_j} and in tangential directions $\boldsymbol{\varepsilon}_{T_j} = (\varepsilon_{B_j}, \varepsilon_{C_j})^\top$ are the so-called tangential coefficient of restitution. The stiffness matrix is abbreviated with \mathbf{K} and \mathbf{q}_0 are the coordinates of the unstressed mechanical model, analogue to the length (l_0) of an unstressed spring in a one-dimensional example. The set C_T is given for spatial isotropic Coulomb friction in Eq. (15). The relative velocity in normal direction of each contact j is calculated at the beginning of the time step $\gamma_{N_j}^A := \gamma_{N_j}(t^A)$ and at its end $\gamma_{N_j}^E := \gamma_{N_j}(t^E)$ as well as the relative velocities in tangential directions $\gamma_{T_j}^A := \gamma_{T_j}(t^A)$ and $\gamma_{T_j}^E := \gamma_{T_j}(t^E)$, respectively (cf. [5, 6]). After solving the inclusion problem the positions at the end of the time step are computed

$$\mathbf{q}^E := \mathbf{q}^A + \frac{1}{2}\Delta t(\mathbf{u}^A + \mathbf{u}^E). \quad (40)$$

In [5] it is described how the procedure in Eq. (37) to Eq. (40) can be reformulated so that it can be solved with a numerical algorithm.

7.2 Implicit integrator

In contrast to an energy consistent integrator (cf. section 7.1) another discretisation of the midpoint position and the endpoint velocity (cf. Eq. (38) and Eq. (40))

$$\mathbf{q}^M := \mathbf{q}^A + \frac{1}{2}\Delta t \mathbf{u}^E, \quad (41)$$

$$\mathbf{q}^E := \mathbf{q}^A + \Delta t \mathbf{u}^E \quad (42)$$

is implemented. The procedure for computing the solution of the inclusion problem is identical to the one described in section 7.1.

8 SIMULATION RESULTS

Fig. 9 shows a simulation for which the cuboid is dropped on the cube, these are the first results of the investigation of the two integration schemes and their differences and the possibilities. The system was computed twice with identical model inputs (e.g. boundary conditions, initial position and velocity, time step size and material data (cf. Tab. 1)). The black lines show the result of the energy consistent integrator and the computed solution of the implicit integrator is red. The aim of the left diagram of Fig. 9 is to depict the different numerical solutions of the

degrees of freedom	DOF = 36
coefficient of restitution	$\varepsilon = 0$
friction coefficient	$\mu = 1.0$
dimension cuboid	$V = 10 \cdot 10 \cdot 5 \text{ mm}^3$
dimension cube	$V = 20 \cdot 20 \cdot 20 \text{ mm}^3$
Young's modulus cuboid	$E = 210 \text{ MPa}$
Young's modulus cube	$E = 210 \text{ GPa}$
Poisson's ratio	$\nu = 0.3$
simulated time	$t = 0.5 \text{ s}$
time step size of simulation	$\Delta t = 10^{-6} \text{ s}$

Table 1: Model data.

two implemented integrators. The interaction of the two bodies on each other is also shown in the same graph with the z-coordinate of node n_1 and n_{13} (cf. Fig. 5). The right graph shows the velocity of node n_1 in z-direction. For a better visualisation of the interaction of both blocks the

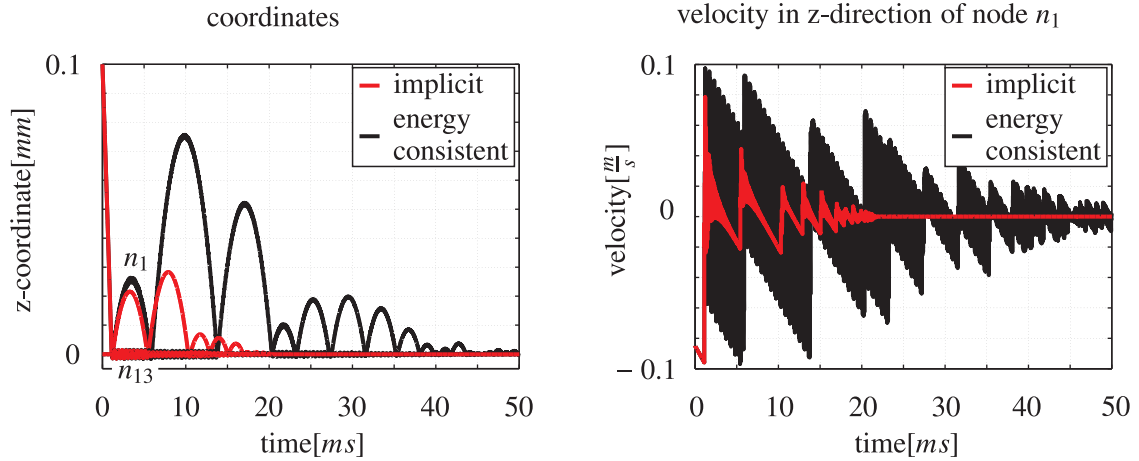


Figure 9: Numerical results: position and velocity.

trajectories of nodes n_1 and n_{13} (cf. left graph of Fig. 9) are printed in detail for each integrator. Fig. 10 depicts the position of the nodes n_1 and n_{13} in case of an integration with the implicit time discretisation (c.f. section 7.2). For both nodes n_1 and n_{13} the solution computed with the energy consistent integrator is shown in Fig. 11. It becomes clear, that the choice of the integrator type has a great influence on the results. The advantage of the shorter computation time of an implicit integrator, which is achieved by a larger time step, has the disadvantage, that the velocity graphs look similar, but they are not identical (cf. Fig. 9 right graph). A comparison of the damped velocity signal (i.e. the implicit integrator scheme) after the first impact e.g. $t = 4 \text{ ms}$ with the computed solution of the energy consistent integrator shows that the resulting velocity in z-coordinate direction (i.e. center of mass velocity without vibrations) is for the use of the implicit integrator smaller than in case of the usage of the energy consistent integrator. For an identical time step as used for the simulations the disagreement of the solutions can be monitored.

Vibrations of the cube and the cuboid, excited due to impacts, can be observed in both numeri-

implicit integrator: coordinates of n_1 and n_{13}

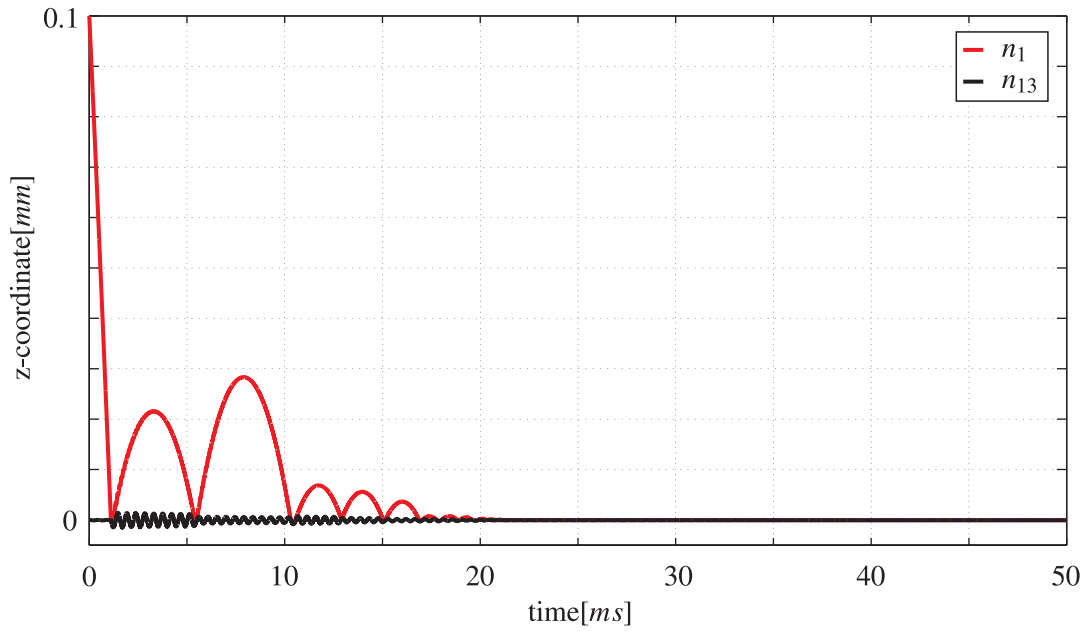


Figure 10: Implicit integrator: numerical position results of node n_1 and n_{13} .

energy consistent integrator: coordinates of n_1 and n_{13}

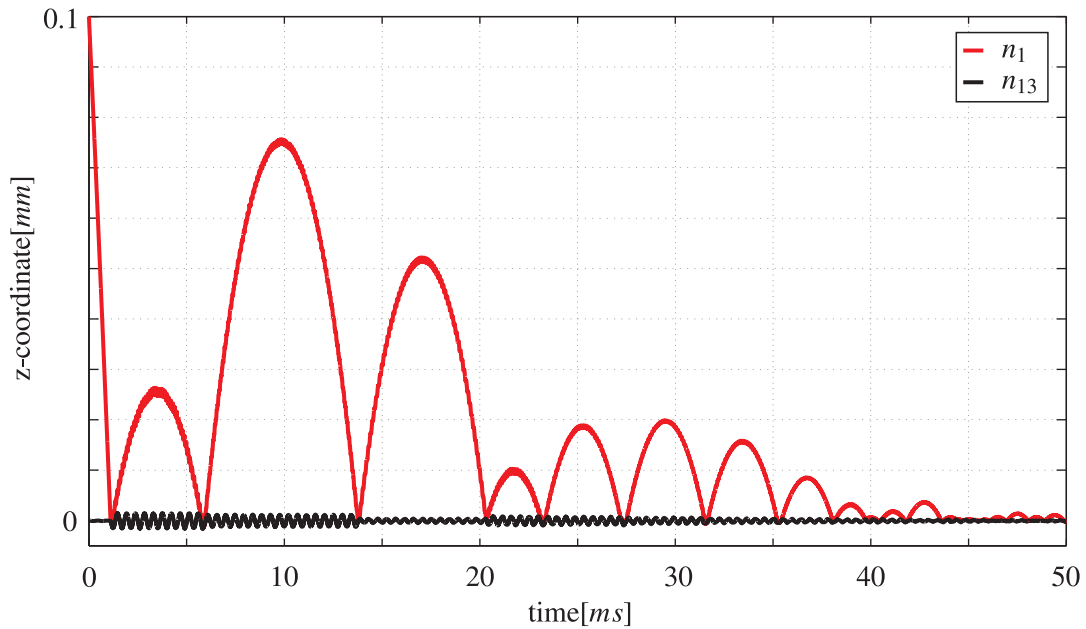


Figure 11: Energy consistent integrator: numerical position resultsof node n_1 and n_{13} .

cal results; on positon level (cf. Fig. 10 and Fig. 11) and on velocity level depicted in the right graph of Fig. 9. The cuboid bounces on the cube and the contacts are closed for several time steps. The collision phases are very short and cannot be discerned.

The changes of the contact area, which is the surface area on the top surface of the cube which is covered by the cuboid in case of contact, is determined for the first collision phases. This is the time period T from $t = 1.11 \text{ ms}$ to $t = 1.15 \text{ ms}$ (cf. Fig. 9). During this time period T the contacts remain closed. It is taken the mean of the changes of the contact area during time period T . If an arbitrary single point in time is chosen out of the time interval T , the result and its interpretation will be meaningless, because the results and interpretations depend on the choice of the instant of time, i.e. the deformation of the blocks can have a positive or negative sign. This fact results from the vibrations of the cube and the cuboid. The results of the changes of the surface areas of both bodies are shown in Fig. 12. The undeformed area of the surfaces, which are part of the node-to-surface contact definition, are printed as continuous lines, the deformed enlarged surface areas of the two blocks are visualised as dot-dashed lines in case of friction and as dashed lines without friction (cf. Fig. 12). The changes of the surface area of the cuboid

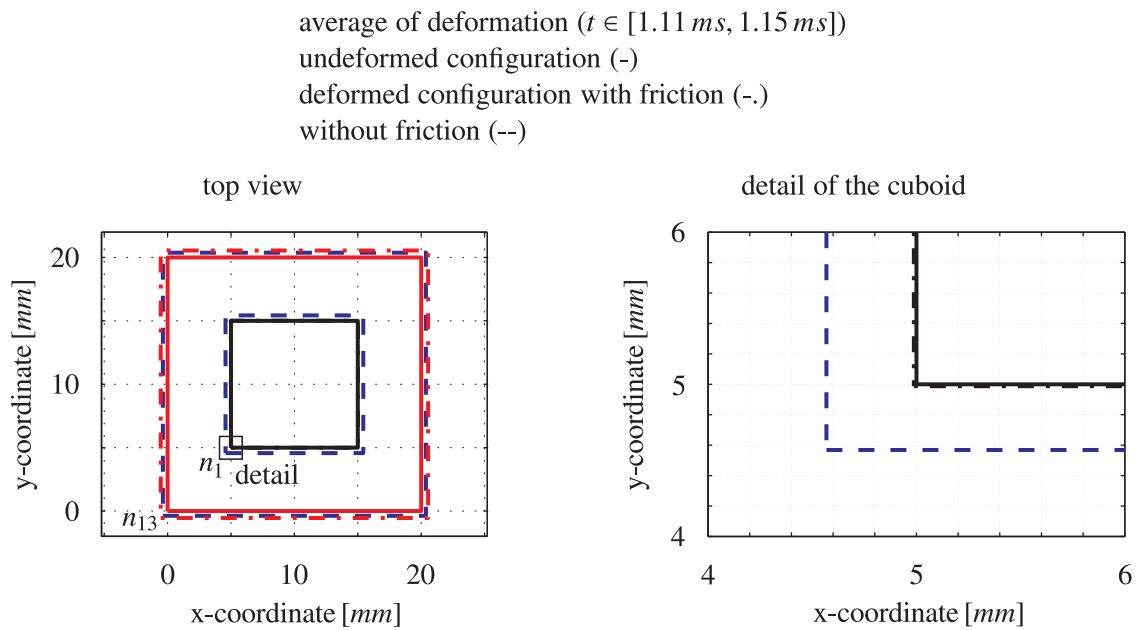


Figure 12: Numerical results: Deformation and contact surface area changes.

are small. A detail of the cuboid at node n_1 is depicted in the right graph of Fig. 12. Different changes of the contact surface area due to the effect of friction can be identified. In frictionless case the upper surface area of the cube, where the contact happens, is less than in case with friction. The detail of the cuboid (cf. Fig. 12 right graph) shows, that the bottom surface area of the cuboid without friction is greater than the one when friction is taken into account. In general case of a collision the cuboid hits the top surface of the cube and both blocks get deformed in z -coordinate direction (cf. Fig. 5). A linear elastic constitutive law is implemented for both blocks, i.e. the deformation in z -direction is coupled with the lateral extension (x, y -directions) of the material via Poisson's ratio ν . The lateral extensions of the cuboid and the cube will not be independent on the contact surface if the coefficient of friction is non-zero. The forces in lateral directions can be submitted via friction. On the one hand the extensions of the cuboid are limited by the contact friction forces, on the other hand the extension of the cuboid can be transmitted to the cube and enlarge its contact surface area. The situation is inverted for the cube. In case without friction the extensions in lateral directions of the cube are only the result

of the coupled deformations in z -direction and lateral directions of the cube. When friction is taken into account the enlargement of the upper surface area of the cube is composed of the coupled deformation, as in frictionless case, and the submitted displacements of the deformed cuboid. That means a greater upper surface area of the cube in case of contact and friction than in case friction is neglected. The results can be summarised as shown in Tab. 2.

	$\mu = 0$	$\mu \neq 0$
expansion cube	less	more
expansion cuboid	more	less
contact area between bodies	more	less

Table 2: Summary of the simulation results.

The main difference is that the cube and the cuboid can interact with each other in case of friction, in case friction is neglected their dynamical behaviour in x, y -direction is independent. Different elastic properties of the materials are the reason for the monitored magnitude of the displacements of the cube and the cuboid surface areas.

9 OUTLOOK

The presented model of two elastic blocks will be the basis for the investigation of vibration phenomena. One of the attentions of further analysis could be self-excited vibrations due to friction. The energy consistent integration scheme seems to have advantages on the field of vibrations analysis. Further investigations of the two different integrators have to be done for a better understanding of their advantages and disadvantages in relation to the scope of investigations of impact and friction phenomena.

REFERENCES

- [1] B. Chetouane, F. Dubois, M. Vinches and C. Bohatier. NSCD discrete element method for modelling masonry structures. *International Journal for Numerical Methods in Engineering*, **64**, 65–94, 2005.
- [2] Ch. Glocker *Dynamik von Starrkörpersystemen mit Reibung und Stößen*. VDI-Fortschrittsberichte Mechanik/Bruchmechanik, Reihe 18, Nr. 182, VDI-Verlag, Düsseldorf 1995.
- [3] Ch. Glocker. Concepts for modeling impacts without friction. *Acta Mechanica*, **168**, 1–19, Springer Verlag, 2004.
- [4] Ch. Glocker. An Introduction to Impacts. *CISM Courses and Lectures*, **485** (eds. J. Haslinger, G. Stavroulakis), 45–102, Springer Verlag, Wien, New York 2006.
- [5] Ch. Glocker. Simulation von harten Kontakten mit Reibung - Eine iterative Projektionsmethode. *Schwingungen in Antrieben, Fulda 2006*, **VDI-Berichte Nr. 1968**, 19–44, VDI-Verlag, Düsseldorf 2006.
- [6] Ch. Glocker, E. Cataldi-Spinola, R.I. Leine. Curve squealing of trains: Measurement, modelling and simulation. *Journal of sound and vibration*, **324**, 362–386, 2009.

- [7] T. J. R. Hughes *The Finite Element Method: Linear Static and Dynamic Finite Element Analysis*. Dover Publications, New York 2000.
- [8] T.A. Laursen and J.C. Simo. A continuum-based finite element formulation for the implicit solution of multibody, large deformation frictional contact problems. *International Journal for Numerical Methods in Engineering*, **36**, 3451–3485, 1993.
- [9] R.I. Leine, H. Nijmeijer *Dynamics and Bifurcations of Non-Smooth Mechanical Systems*. Volume 18 of Lecture Notes in Applied and Computational Mechanics, Springer, Berlin 2004.
- [10] M. Möller *Consistent Integrators for non-smooth dynamical systems*. PhD thesis, ETH Zürich, to be published in 2011.
- [11] J.J. Moreau. Unilateral contact and dry friction in finite freedom dynamics. *CISM Courses and Lectures*, **302** (eds. J.J. Moreau, P.D. Panagiotopoulos), 1–82, Springer Verlag, Wien 1988.
- [12] O.C. Zienkiewicz and R.L. Taylor *THE FINITE ELEMENT METHOD Volume 1 The Basis Fifth Edition*. Butterworth Heinemann, Oxford 2000.